Huge splitting of polariton states in microcavities under stress

R. Balili,* B. Nelsen, and D. W. Snoke†
Department of Physics and Astronomy, University of Pittsburgh, 3941 O'Hara Street, Pittsburgh, Pennsylvania 15260, USA

R. H. Reid
Mechanical Engineering Department, Carnegie Mellon University, 5000 Forbes Avenue, Pittsburgh, Pennsylvania 15213, USA

L. Pfeiffer‡ and K. West‡
Bell Labs, Lucent Technologies, 700 Mountain Avenue, Murray Hill, New Jersey 07974, USA

(Received 30 July 2009; revised manuscript received 27 January 2010; published 10 March 2010)

The application of inhomogeneous stress, used to trap polaritons in a microcavity, results in a splitting between different polarization states of the polaritons. The splitting of the polariton states arises primarily from the splitting of the exciton states in the quantum wells embedded inside the microcavity due to the electron-hole exchange interaction and the mixing of the light- and heavy-hole excitons with stress. The new mixed exciton states have different oscillator strengths, thereby enhancing the splitting of the lower polaritons by a factor of four more than previously reported exciton spin splittings. We observe splittings between the different polarizations, at normal incidence, of almost 1 meV. The physical explanation and a corresponding simulation for the fine structure splitting of the polaritons observed in stressed microcavities are presented.

DOI: 10.1103/PhysRevB.81.125311 PACS number(s): 78.67.−n, 71.35.Lk, 71.36.+c, 03.75.Nt

Microcavities with embedded quantum wells, which produce exciton-polariton states in the strong coupling limit, are an active topic of experimental and theoretical research,[1–7] in particular, in regard to the recent demonstrations of nonequilibrium Bose condensation.[8–18] In our recent experiments with GaAs-based structures, inhomogeneous stress was used to create a harmonic potential to confine the polaritons.[9,19] One extra effect of the stress is that it leads to a splitting of the two polarization states of the polaritons. For moderate stresses, this splitting can be huge compared to typical exciton splittings in GaAs quantum wells. In this paper, we explore in detail the mechanisms which lead to this splitting.

For the experiments, three sets of four identical 70-Å GaAs quantum wells were placed at the three antinodes of the confined optical mode in a microcavity. The design, which uses two GaAs/AlGaAs-distributed Bragg reflectors to create the cavity, is essentially the same one as used in previous experiments.[9,16,20] The coupling between the exciton states and the photon states gives rise to polariton states which are superpositions of excitons and photons. Initially, there are four nearly-degenerate exciton states, with two bright ($J=\pm 1$) states and two dark ($J=\pm 2$) states split by about 150 μeV.[21,22] When the bright excitons couple to the two photon states, two polariton states are shifted down relative to the original exciton states and two are shifted upward, while the dark exciton states are left nearly unaffected. The Q factor of the cavity in our samples is around 4000 and the Rabi splitting between the upper and lower polariton states is about 15 meV, compared to typical line widths of the lower polaritons of 0.25 meV. Stress was applied by a sharp pin to the backside of the substrate of a freely suspended sample, as in previous experiments.[9,19] A minimum in the band gap is created in the quantum wells at a point in the plane just below the pin stressor. This energy minimum corresponds to the center of the trap and can be approximated as a harmonic potential for the polaritons in the plane of their motion.

A state splitting of up to 700 μeV is observed in the lower and upper polariton branches of a stressed semiconductor microcavity polariton. The split states are linearly polarized and orthogonal to each other. In addition, one of the states couples to light better than the other as seen by the difference in the Rabi splitting of the upper and lower polaritons. Typical spectra are shown in Fig. 1.

An example of the splitting of the lower polariton state in a line across the stress trap is shown in Fig. 2. The difference in energy between two bright states is extracted from photoluminescence measurements taken normal to the sample and is plotted in Fig. 3(b). The range of stress for the data of Fig. 3(b) are taken from close to zero detuning to positive detuning ($\delta=E_{ph}-E_{ex}$). Normal to the sample, the transverse electric and transverse magnetic modes in the cavity are

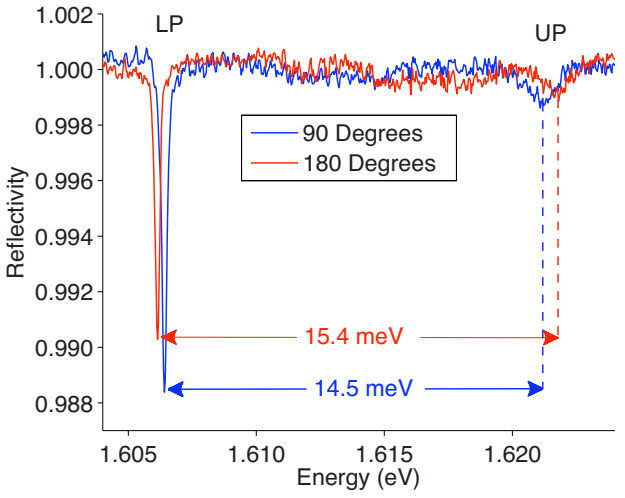

FIG. 1. (Color online) An example of the refectivity spectra of the polariton through a 90° and a 180° polarizer orientation. The spectra are taken 150 μm away from the center of the stress well.

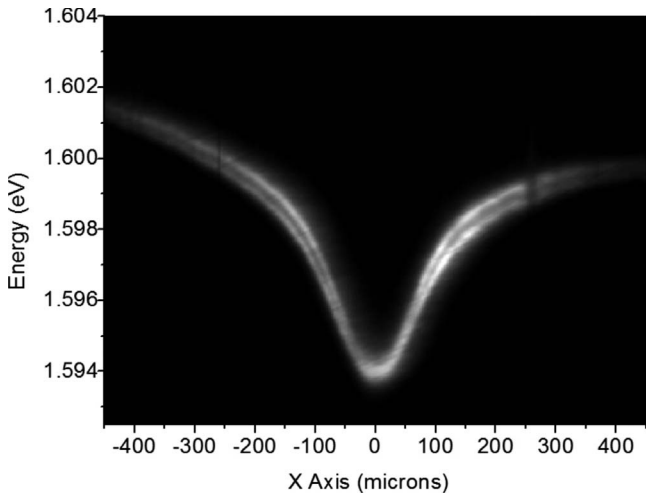

FIG. 2. An example of the lower polariton luminescence showing the splitting of the two bright states across a stressed microcavity sample (4.3 N force on the pin stressor; see Refs. 9 and 23 for the stressor geometry).

equivalent. Hence, the longitudinal-transverse splitting of polaritons does not contribute to the splitting. The splitting could arise from two possibilities. One is that it could be a direct effect of an energy splitting of the degenerate bright exciton states (spin ± 1) into two orthogonally-polarized radiative states. Another possibility is that it could be due to a stress-induced birefringence in the microcavity, resulting in a splitting of the bare photon mode into two polarized states. However, the photonic character is not enhanced in our case since the polariton becomes more excitonlike with increasing stress.[16,24] It is safe to assume that the splitting caused by a small birefringence in the mirrors and cavity is not the dominant cause.

Exciton splitting due to exchange anisotropy is well studied in GaAs quantum wells and microcavities.[22,25–30] The energy splittings between the bright states in quantum wells are typically at most a few tens of μeV.[22] In unstressed samples, the mixing between heavy-hole and light-hole excitons is negligible since they are far apart in energy ($\sim$30 meV difference for 7-nm quantum wells). In our experiments,[23] the stress shifts the light-hole energy close to the heavy-hole energy, making the mixing between the two states an important parameter to consider.

The breaking of the degeneracy of the two bright excitonic states is the result of a lowering of the symmetry that can be induced by external strain, inherent and induced piezoelectric fields, and/or interface roughness possibly linked to the growth procedures.[27,30,31] This would mean a reduction in the symmetry of the QW from D_{2d} to C_{2v}.[30] Therefore, the [110] and $[1\bar{1}0]$ axes are no longer equivalent, splitting the exciton states into orthogonal, linearly polarized states. In the D_{2d} symmetry group, both the conduction spin-1/2 states and valence $j=3/2$ states are represented by Γ_6. The product gives

$$\Gamma_6 \otimes \Gamma_6 = \Gamma_1 \oplus \Gamma_2 \oplus \Gamma_5.$$

The representations Γ_1 and Γ_2 correspond to the dipole-inactive $J=\pm 2$ states and the Γ_5 corresponds to the dipole-active $J=\pm 1$ states. When the symmetry is lowered to C_{2v}, the Γ_5 doublet becomes $\Gamma_2 \oplus \Gamma_4$, which are optically-active x and y singlet states.

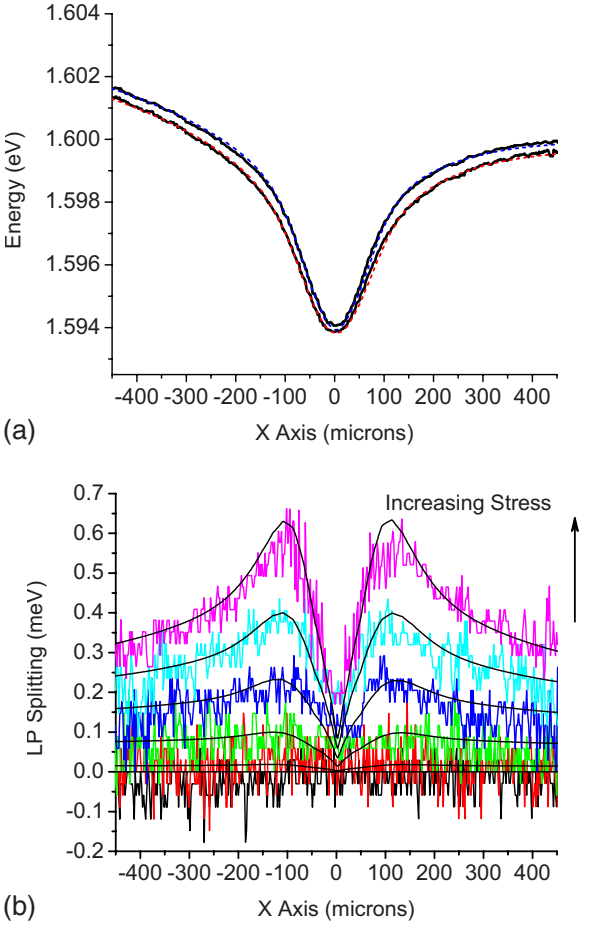

FIG. 3. (Color online) (a) Solid black lines: the peak position of the data of Fig. 2. Colored dashed lines: fit to the data using the full Pikus-Bir and exchange Hamiltonian discussed in the text. (b) Measured splitting between the lower polariton states with increasing force on the pin stressor (0, 0.2, 1.0, 2.1, 3.2, and 4.3 N). The highest stress splitting corresponds to the difference in the curves in Fig. 2. The solid curves are fits of the theory discussed in the text.

When the symmetry is lowered, it is natural to expect the exciton oscillator strength to also be different along the two crystal axis orientations.[30] Each polarization will then have a different Rabi splitting. In fact, the change in oscillator strength is a big factor in creating these huge polariton splittings, up to 700 μeV as seen in our experiments, since the polariton splitting amplifies the spin splitting. The polariton energies for a given exciton state are found by diagonalizing the matrix

$$H = \begin{pmatrix} E_i & \Omega_i \\ \Omega_i & E_{\text{photon}} \end{pmatrix}, \tag{1}$$

where Ω_i is the radiative coupling for exciton eigenstate i, which depends on the relative fraction of light-hole and heavy-hole excitons in the eigenstate.

TABLE I. Relevant parameters used for the Pikus-Bir and exchange Hamiltonian fit shown in Fig. 3(a).

Hole diameter	1.25 mm
Pin diameter	25 μm
Relevant parameters for GaAs/AlGaAs:	Refs. 34 and 35
Exchange coupling terms $a_x=a_y$	1.14 meV
a_z	0.84 meV
Bare heavy-hole radiative coupling Ω_{hh}	7.55 meV
Bare light-hole radiative coupling Ω_{lh}	6.0 meV

The Hamiltonian that can split the degeneracy of the two bright states is the short-range electron-hole exchange interaction between a hole with spin S_h and an electron with spin S_e.[32]

$$H_{exch} = -\sum_{i=x,y,z} a_i S_{h,i} S_{e,i}, \tag{2}$$

where the a's are the coupling constants. Anisotropy in the exchange interaction is enough to split the degeneracy of the exciton states but anisotropy is not a necessary condition if there is a strong mixing between the light- and heavy-hole excitons, which is the case of our stressed microcavity sample. Adding the Pikus-Bir deformation Hamiltonian, which determines the shift of the bands with stress, to the exchange term and diagonalizing the resulting Hamiltonian matrix leads to a splitting of the exciton energy and a difference in the coupling strength of the new states. (Details are given in Appendix A; Bayer *et al.*[33] used a slightly different form of the short-range exchange interaction; the form used here is justified in Appendix B.) From the resulting exciton eigenstates and their corresponding coupling strengths to the cavity photon, we can solve for the energy of new lower polariton states. For our fits to the data, we assume that the oscillator strength of the pure $J=1$ heavy-hole exciton and the pure $J=1$ light-hole exciton remain constant, but as the stress changes the relative fraction of heavy-hole and light-hole states in each of the two new exciton eigenstates, the oscillator strength of each exciton state must be recomputed.

The splitting in energies of the bright states using the Pikus-Bir plus exchange Hamiltonian for the exciton eigenstates and then the polariton energy splitting using the calculated light-hole and heavy-hole fractions, is compared to the data in Fig. 3(b). The data is well fit using strain values, ε_{xx}, ε_{yy}, etc., for a line across the sample 25 μm off the center of the pin stressor and in the direction of the [100] axis. The relevant parameters used are listed in Table I. The Rabi splitting Ω is proportional to the square root of the calculated oscillator strength $|\langle f|M|i\rangle|^2$, where the final states are the ± 1 spin photons and the inital states are the new eigenstates.

From the eigenvectors of the effective Hamiltonian (Pikus-Bir plus exchange), we can determine the direction of polarization of the exciton. One can write a general representation of the exciton polarization as

$$\mathbf{P}(\mathbf{x}) = (A_+\omega^+ + A_-\omega^-), \tag{3}$$

where $A_+(A_-)$ are the amplitudes of right (left) circularly polarized excitons $\omega_+(\omega_-)$ corresponding to the sum of eigenvector elements with $+1(-1)$ spin. If the magnitude of the amplitudes are equal, $r=|A_-|/|A_+|=1$, then the polarization is 100% linear. For circular components with equal amplitude, it is easy to show that

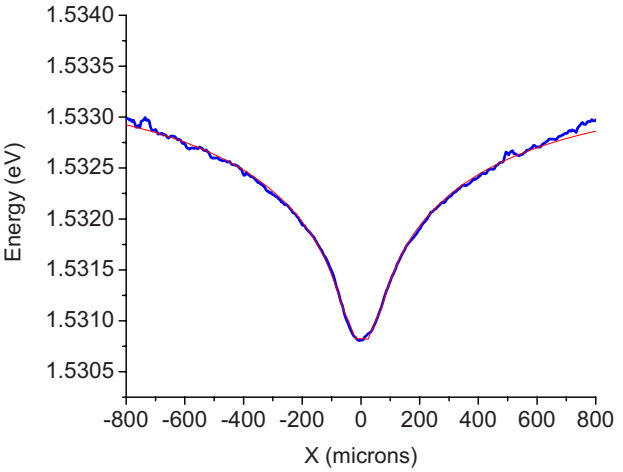

FIG. 4. (Color online) Example of a fit using strain simulations from ANSYS (thin line, in red) on an the single-quantum-well exciton energy of a stressed double quantum well (heavy line, in blue), for 0.7 N force on pin stressor, for an experiment similar to a work done previously (Ref. 19). The following book values (e.g., Ref. 34) for the deformation potentials for GaAs were used for these fits: $a_c=-7.17$ eV, $a_v=1.16$ eV, $b=-1.7$ eV, and $d=-4.55$ eV.

$$\tan\theta = \frac{A_-\omega^-}{A_+\omega^+} = \frac{\omega^-}{\omega^+}, \tag{4}$$

$$\theta = \frac{\alpha}{2}, \tag{5}$$

where the circular polarization is a superposition of linear polarizations along the [100] and [010] axes, $\omega_\pm = \frac{1}{\sqrt{2}}(\epsilon_1 \pm i\epsilon_2)$, α is the phase difference between the amplitudes, $A_-/A_+ \propto e^{i\alpha}$, and θ is the direction of polarization with respect to the [100] axis. Calculating r and θ from our simulations shows that the polarization is nearly 100% linear and points effectively in the [110] and the $[1\bar{1}0]$ directions, for lower polaritons near the center of the trap. In our earlier paper,[9] we presented evidence of optical anisotropy in which the emission is linearly polarized and pinned to one of the [110] crystallographic axis above the condensation density threshold. We believe that this effect can be attributed to the anisotropy explained here.

These experiments provide an unusual degree of accuracy for the electron-hole exchange parameters because the microcavity makes the spin splitting of the different eigenstates much larger than their line widths. The sensitive dependence of the spin splitting on stress also makes this a tool for measuring stress optically that does not depend on the intensity of the lines.

In addition, the splitting due to the stress trap removes the degeneracy of the ground state everywhere except at the exact center of the trap. This may be a crucial factor in the reported observation of a Bose-Einstein condensate in micro-

cavity polaritons[9,16] as compared to unstressed systems.[15] If the ground state is degenerate, the total number of particles in the ground state is divided equally among the degenerate states. This effectively increases the critical density threshold for Bose condensation by a factor of two.

ACKNOWLEDGMENTS

This work has been supported by the National Science Foundation under Grant No. DMR-0706331. We thank J. Wuenschell for contributions to the strain calculations.

APPENDIX A: HAMILTONIAN FOR THE VALENCE-BAND STATES

The valence-band energy shifts as a function of stresses are given by the Pikus-Bir deformation Hamiltonian:[36]

$$H_{PB} = a_v(\epsilon_{xx} + \epsilon_{yy} + \epsilon_{zz}) + b[(J_x^2 - J^2/3)\epsilon_{xx} + c\,.\,p.] + \frac{2d}{\sqrt{3}}\left[\frac{1}{2}(J_xJ_y + J_yJ_x)\epsilon_{xy} + c\,.\,p.\right], \tag{A1}$$

where a_v, b, and d are deformation potentials, ϵ_{ij}'s are stress-tensor components, J's are the angular momentum operators acting on the spin states of the valence band ($m=3/2$, $1/2$, $-1/2$, and $-3/2$), and $c.p.$'s correspond to cyclic permutations with respect to x, y, z. Relevant material properties used in our simulations, e.g., deformation potentials and elastic constants, are found in Refs. 34, 35, and 37. Acting on the heavy-hole and light-hole basis, $|\frac{3}{2},\frac{3}{2}\rangle$, $|\frac{3}{2},\frac{1}{2}\rangle$, $|\frac{3}{2},-\frac{1}{2}\rangle$, $|\frac{3}{2},-\frac{3}{2}\rangle$, Eq. (A1) gives the matrix form[34,38] of the Pikus-Bir Hamiltonian

$$H_{PB} = -\begin{pmatrix} P+Q & -S & R & 0 \\ -S^* & P-Q & 0 & R \\ R^* & 0 & P-Q & S \\ 0 & R^* & S^* & P+Q \end{pmatrix}, \tag{A2}$$

where

$$P = -a_v(\varepsilon_{xx} + \varepsilon_{yy} + \varepsilon_{zz}), \quad Q = -\frac{b}{2}(\varepsilon_{xx} + \varepsilon_{yy} - 2\varepsilon_{zz}),$$

$$R = \frac{\sqrt{3}}{2}b(\varepsilon_{xx} - \varepsilon_{yy}) - id\varepsilon_{xy}, \quad S = -d(\varepsilon_{xz} - i\varepsilon_{yz}).$$

Diagonalizing this the matrix gives the shift of the valence-band energies. The shift of the conduction band is given simply by $\Delta E_c = a_c(\varepsilon_{xx}+\varepsilon_{yy}+\varepsilon_{zz})$.

To be able to diagonalize H_{PB} throughout the sample, we need the values for the strain at different points on the sample as we stress it (see Refs. 19 and 23 for the stressor geometry). The strain terms, ε_{xx}, ε_{yy}, etc., can be computed using programs that use finite-element analysis, e.g., ANSYS. Finite-element analysis numerically calculates the displacements of a discretized mesh representation of the sample using the constitutive relations of GaAs.[38] We begin by calculating the equilibrium displacement of the mesh points by solving Newton's law for continuous media. Following notation from Ref. 38, we have

$$\sum_j \frac{\partial \sigma_{ij}}{\partial x_j} = \rho \ddot{u}_i, \tag{A3}$$

where ρ is the density of GaAs and u_i is the diplacement of a volume element in the i direction. Combining this with Hooke's law, $\sigma_{ij} = \Sigma_{lm} C_{ijlm}\varepsilon_{lm}$, we get

$$\rho \ddot{u}_i = \sum_{jlm} C_{ijlm}\frac{\partial^2 u_l}{\partial x_j\,\partial x_m}, \tag{A4}$$

where we define

$$\varepsilon_{lm} = \frac{1}{2}\left(\frac{\partial u_l}{\partial x_m} + \frac{\partial u_m}{\partial x_l}\right).$$

Equation (A4) is discretized and applied to all points of the constructed mesh representation of the sample when doing the actual simulation. A force on the stressor pin, for example, corresponds to a displacement of the mesh points under the stressor. The right-hand side of Eq. (A4) calculates the force felt by the other mesh points due to the initial displacement. The next iteration then is a displacement of each mesh point in the same direction as force with magnitude proportional to the force felt by each point. After the displacement, the force is again calculated. The process repeats until equilibrium is reached. From the equilibrium displacements (u_i's), one can calculate the strain terms, ε_{xx}, ε_{yy}, etc., that go into H_{PB}. Figure 4 shows a typical calculation of the exciton energy in a quantum well using ANSYS for the strains and book values for the deformation potentials.

The Hamiltonian that can split the degeneracy of the two bright states is the short-range electron-hole exchange interaction between a hole with spin S_h and an electron with spin S_h (Ref. 32)

$$H_{exch} = -\sum_{i=x,y,z} a_i S_{h,i} S_{e,i}, \tag{A5}$$

where the a's are the coupling constants (see Appendix B for the derivation of this term). Acting on the hole-electron basis, $|\frac{3}{2}\rangle|\uparrow\rangle$, $|\frac{3}{2}\rangle|\downarrow\rangle$, $|\frac{1}{2}\rangle|\uparrow\rangle$, $|\frac{1}{2}\rangle|\downarrow\rangle$, $|-\frac{1}{2}\rangle|\uparrow\rangle$, $|-\frac{1}{2}\rangle|\downarrow\rangle$, $|-\frac{3}{2}\rangle|\uparrow\rangle$, and $|-\frac{3}{2}\rangle|\downarrow\rangle$, this is

$$-\begin{pmatrix}
\frac{a_z}{4} & 0 & 0 & \frac{-(a_x-a_y)}{\sqrt{3}} & 0 & 0 & 0 & 0 \\
0 & -\frac{a_z}{4} & \frac{-(a_x+a_y)}{\sqrt{3}} & 0 & 0 & 0 & 0 & 0 \\
0 & \frac{-(a_x+a_y)}{\sqrt{3}} & \frac{a_z}{12} & 0 & 0 & \frac{2(a_x-a_y)}{3} & 0 & 0 \\
\frac{-(a_x-a_y)}{\sqrt{3}} & 0 & 0 & -\frac{a_z}{12} & \frac{2(a_x+a_y)}{3} & 0 & 0 & 0 \\
0 & 0 & 0 & \frac{2(a_x+a_y)}{3} & -\frac{a_z}{12} & 0 & 0 & \frac{-(a_x-a_y)}{\sqrt{3}} \\
0 & 0 & \frac{2(a_x-a_y)}{3} & 0 & 0 & \frac{a_z}{12} & \frac{-(a_x+a_y)}{\sqrt{3}} & 0 \\
0 & 0 & 0 & 0 & 0 & \frac{-(a_x+a_y)}{\sqrt{3}} & -\frac{a_z}{4} & 0 \\
0 & 0 & 0 & 0 & \frac{-(a_x-a_y)}{\sqrt{3}} & 0 & 0 & \frac{a_z}{4}
\end{pmatrix}. \tag{A6}$$

The exchange term is added to the Pikus-Bir deformation matrix to account for the shift of the bands due to both exchange and deformation. The Pikus-Bir Hamiltonian, acting in the same basis state as the exchange, is

$$H_{PB} = -\begin{pmatrix}
P+Q & 0 & -S & 0 & R & 0 & 0 & 0 \\
0 & P+Q & 0 & -S & 0 & R & 0 & 0 \\
-S^* & 0 & P-Q & 0 & 0 & 0 & R & 0 \\
0 & -S^* & 0 & P-Q & 0 & 0 & 0 & R \\
R^* & 0 & 0 & 0 & P-Q & 0 & S & 0 \\
0 & R^* & 0 & 0 & 0 & P-Q & 0 & S \\
0 & 0 & R^* & 0 & S^* & 0 & P+Q & 0 \\
0 & 0 & 0 & R^* & 0 & S^* & 0 & P+Q
\end{pmatrix}. \tag{A7}$$

Diagonalizing $H_{PB}+H_{exch}$ at every point of a numerically discretized mesh of GaAs gives the shifted band energies with stress.

The heavy-hole excitons are those with the valence-band 3/2 states while the light-hole excitons are those with the valence-band 1/2 states. Only the states with $J=1$ are bright states, i.e., states $|\frac{3}{2}\rangle|\downarrow\rangle$ and $|-\frac{3}{2}\rangle|\uparrow\rangle$ for the heavy hole excitons, and states $|\frac{1}{2}\rangle|\uparrow\rangle$ and $|-\frac{1}{2}\rangle|\downarrow\rangle$ for the light hole excitons. The radiative oscillator strength for each eigenstate is proportional to $|\langle \mathrm{vac}|p|i\rangle|^2$, where

$$|i\rangle = \alpha_1|hh,2\rangle + \alpha_2|hh,1\rangle + \alpha_3|lh,1\rangle + \alpha_4|lh,0(a)\rangle + \alpha_5|lh,0(b)\rangle + \alpha_6|lh,-1\rangle + \alpha_7|hh,-1\rangle + \alpha_8|hh,-2\rangle$$

is the eigenstate found in the above electron-hole basis; $\langle \mathrm{vac}|p|hh,\pm 1\rangle = M_{hh}$ and $\langle \mathrm{vac}|p|lh,\pm 1\rangle = M_{lh}$ are fit parameters, and the other matrix elements are zero.

APPENDIX B: DERIVATION OF ELECTRON-HOLE EXCHANGE

To deduce the electron-hole exchange term from first principles we begin by following the method of Hanamura and Haug.[39] The interaction energy is written in terms of the electron Fermi field operators as

$$H = \sum_{s,s'} \int d^3x \int d^3x' \frac{e^2}{4\pi\epsilon|\vec{x}-\vec{x}'|} \psi_s^\dagger(\vec{x})\psi_{s'}^\dagger(\vec{x}')\psi_{s'}(\vec{x}')\psi_s(\vec{x}), \tag{B1}$$

where

$$\psi_s(\vec{x}) = \frac{1}{\sqrt{V}} \sum_{n,\vec{k}} \langle u_{n\vec{k}}|\vec{x},s\rangle e^{i\vec{k}\cdot\vec{x}} b_{n\vec{k}}$$

in which $\langle u_{n\vec{k}}|\vec{x},s\rangle$ is the spin-s projection of the Bloch cell function for an electron with band index n and momentum $\vec{k}$,

and $b_{n\vec{k}}$ and $b^{\dagger}_{n\vec{k}}$ are the fermionic annihilation and creation operators. Substitution gives

$$H = \sum_{\{n,\vec{k}\}} b^{\dagger}_{n\vec{k}} b^{\dagger}_{n'\vec{k}'} b_{n''\vec{k}''} b_{n'''\vec{k}'''} \sum_{s,s'} \int d^3x \int d^3x' \times e^{-i(\vec{k}\cdot\vec{x}+\vec{k}'\cdot\vec{x}'-\vec{k}''\cdot\vec{x}'-\vec{k}'''\cdot\vec{x})} \langle \vec{x},s|u_{n\vec{k}}\rangle\langle \vec{x}',s'|u_{n'\vec{k}'}\rangle\langle u_{n''\vec{k}}|\vec{x}',s'\rangle \times \langle u_{n'''\vec{k}'''}|\vec{x},s\rangle \frac{e^2}{4\pi\epsilon|\vec{x}-\vec{x}'|}, \tag{B2}$$

where the summation over $\{n,\vec{k}\}$ stands for summation over all bands n and momenta $\vec{k}$. We make the long-wavelength approximation that all k's are small compared to the Brillouin zone, which means that the plane-wave terms are nearly constant over a unit cell.[38] We write $\vec{x}=\vec{X}+\vec{y}$, where $\vec{X}$ is the position of a cell and $\vec{y}$ is the position inside a cell, and take the lowest order of the $\vec{k}\cdot\vec{p}$ expansion for the Bloch cell functions,[38] to write

$$\frac{1}{V}\int d^3x e^{-i(\vec{k}-\vec{k}''')\cdot\vec{x}} \langle \vec{x},s|u_{n\vec{k}}\rangle\langle u_{n'''\vec{k}'''}|\vec{x},s\rangle \approx \frac{1}{N}\sum_{\vec{X}} e^{-i(\vec{k}-\vec{k}''')\cdot\vec{X}} \frac{1}{V_{\text{cell}}}\int_{\text{cell}} d^3y \langle \vec{y},s|u_{n0}\rangle\langle u_{n'''0}|\vec{y},s\rangle,$$

where N is the number of unit cells and V_{cell} is the volume of a unit cell. This yields the approximate result

$$H \simeq \sum_{\{n,\vec{k}\}} b^{\dagger}_{n\vec{k}} b^{\dagger}_{n'\vec{k}'} b_{n''\vec{k}''} b_{n'''\vec{k}'''} \frac{1}{N^2}\sum_{X,X'} e^{-i(\vec{k}\cdot\vec{X}+\vec{k}'\cdot\vec{X}'-\vec{k}''\cdot\vec{X}'-\vec{k}'''\cdot\vec{X})} \times \sum_{s,s'} \frac{1}{V_{\text{cell}}^2}\int_{\text{cell}} d^3y \int_{\text{cell}} d^3y' \langle \vec{y},s|u_{n0}\rangle\langle \vec{y}',s'|u_{n'0}\rangle \times \langle u_{n''0}|\vec{y}',s'\rangle\langle u_{n'''0}|\vec{y},s\rangle \frac{e^2}{4\pi\epsilon|\vec{x}-\vec{x}'|}. \tag{B3}$$

The denominator $|\vec{x}-\vec{x}'|$ must be treated with care. We break the sum over $\vec{X}$ and $\vec{X}'$ into two parts, one with $\vec{X}=\vec{X}'$ (short range) and one with $\vec{X}\neq\vec{X}'$ (long range). The latter term is approximately

$$H \simeq \sum_{\{n,\vec{k}\}} b^{\dagger}_{n\vec{k}} b^{\dagger}_{n'\vec{k}'} b_{n''\vec{k}''} b_{n'''\vec{k}'''} \frac{1}{N^2}\sum_{X\neq X'} \times e^{-i(\vec{k}\cdot\vec{X}+\vec{k}'\cdot\vec{X}'-\vec{k}''\cdot\vec{X}'-\vec{k}'''\cdot\vec{X})} \frac{e^2}{4\pi\epsilon|\vec{X}-\vec{X}'|} \times \left(\sum_{s} \frac{1}{V_{\text{cell}}}\int_{\text{cell}} d^3y \langle \vec{y},s|u_{n0}\rangle\langle u_{n'''0}|\vec{y},s\rangle\right) \times \left(\sum_{s'} \frac{1}{V_{\text{cell}}}\int_{\text{cell}} d^3y' \langle \vec{y}',s'|u_{n'0}\rangle\langle u_{n''0}|\vec{y}',s'\rangle\right). \tag{B4}$$

The sum over $\vec{X}$ and $\vec{X}'$ can be converted to an integral and resolved as[38]

$$\frac{1}{2V}\frac{e^2/\epsilon}{|\Delta k|^2}\delta_{k+k',k''+k'''},$$

where $\Delta k=\vec{k}-\vec{k}'''=\vec{k}''-\vec{k}'$. For $n=n'''$ and $n'=n''$, this term gives the standard intraband Coulomb interaction, either between two carriers in the same band, or in the case of an electron and hole, the direct Coulomb interaction between an electron and hole that causes exciton formation. The long-range exchange term vanishes in the long-wavelength limit assumed here due to the orthonormality of the Bloch cell functions; higher-order $\vec{k}\cdot\vec{p}$ expansion of the Bloch cell functions will give a k-dependent term.

On the other hand, the short-range term has a matrix element

$$\langle U_{n,n',n'',n'''}\rangle = \sum_{s,s'} \frac{1}{V_{\text{cell}}^2}\int_{\text{cell}} d^3y \int_{\text{cell}} d^3y' \langle \vec{y},s|u_{n0}\rangle\langle \vec{y}',s'|u_{n'0}\rangle \times \langle u_{n''0}|\vec{y}',s'\rangle\langle u_{n'''0}|\vec{y},s\rangle \frac{e^2}{4\pi\epsilon|\vec{y}-\vec{y}'|}, \tag{B5}$$

which can be nonzero for Bloch cell functions in different bands. To determine the exchange energy for an exciton, we use the Wannier exciton state, written as

$$|cv\rangle = \sum_{\vec{k}} \phi(\vec{k}) b^{\dagger}_{c\vec{k}} b_{v\vec{k}},$$

where c and v are indices that pick out specific conduction and valence-band states, respectively, and $\phi(\vec{k})$ is the momentum-space wave function of the relative exciton motion (we assume that the center-of-mass motion of the exciton is negligible). The exchange energy is then given by

$$\langle ex|H|ex\rangle \simeq \left[\langle 0|\sum_{\vec{p}'} \phi^*(\vec{p}') b^{\dagger}_{v\vec{p}'} b_{c\vec{p}'}\right] \frac{V_{\text{cell}}}{V}\langle U_{cvcv}\rangle \times \sum_{\vec{k},\vec{k}',\vec{q}} b^{\dagger}_{c,\vec{k}} b^{\dagger}_{v,\vec{k}'} b_{c,\vec{k}'+\vec{q}} b_{v,\vec{k}-\vec{q}} \left[\sum_{\vec{p}} \phi(\vec{p}) b^{\dagger}_{c\vec{p}} b_{v\vec{p}}|0\rangle\right], \tag{B6}$$

where the sum over $\vec{X}$ $(=\vec{X}')$ has been used to give a momentum-conserving δ function. When all the creation and annihilation operators are resolved into constraints on the momentum vectors, this becomes,

$$\langle ex|H|ex\rangle \simeq -\left(\sum_{\vec{p}'} \phi^*(\vec{p}')\right)\frac{V_{\text{cell}}}{V}\langle U_{cvcv}\rangle\left(\sum_{p} \phi(\vec{p})\right) + \left(\sum_{p} |\phi(\vec{p})|^2\right)\frac{V_{\text{cell}}}{V}\langle U_{cvcv}\rangle \simeq -|\varphi(0)|^2 V_{\text{cell}}\langle U_{cvcv}\rangle, \tag{B7}$$

where we have found the real-space exciton wave function through the the Fourier transform $\varphi(\vec{r})=(1/\sqrt{V})\Sigma_k \phi(k) e^{i\vec{k}\cdot\vec{r}}$; the second term in the first line of Eq. (B7) is negligible since the wave function is normalized so this term is of order $1/V$ times the first term. The short-range exciton exchange energy is therefore proportional to the probability of the elec-

tron and hole in the exciton Wannier wave function being at the same place.

The matrix element, Eq. (B5), for interband transitions relies on the spatial variation in the Coulomb potential to give a nonzero integral. However, the Coulomb interaction does not flip spin. Therefore, the exchange interaction applies only for electron and hole states with the same spin. Since the case of same spins corresponds to the spin-triplet case and the case of different spins corresponds to the spin-singlet state, in the case of pure spin states, we account for this with a factor $-\vec{S}_e \cdot \vec{S}_h$.[38]

In the case when the conduction-band eigenstates are pure spin states but the valence-band eigenstates are not, as in GaAs, we cannot just worry about the diagonal terms $\langle ex|H|ex\rangle$ for the exciton energy; we must also worry about mixing terms $\langle ex'|H|ex\rangle$, where the exciton states can be different, and the resulting terms $U_{c'v'cv}$. The four relevant GaAs valence band states at zone center are

$$\left|+\tfrac{3}{2}\right\rangle = -i|1\rangle|\uparrow\rangle,$$

$$\left|+\tfrac{1}{2}\right\rangle = \tfrac{i}{\sqrt{3}}|1\rangle|\downarrow\rangle + \tfrac{i\sqrt{2}}{\sqrt{3}}|0\rangle|\uparrow\rangle,$$

$$\left|-\tfrac{1}{2}\right\rangle = \tfrac{i}{\sqrt{3}}|-1\rangle|\uparrow\rangle + \tfrac{i\sqrt{2}}{\sqrt{3}}|0\rangle|\downarrow\rangle,$$

$$\left|-\tfrac{3}{2}\right\rangle = -i|-1\rangle|\downarrow\rangle, \tag{B8}$$

where the states $|1\rangle$, $|0\rangle$ and $|-1\rangle$ are the Bloch spatial cell functions with p symmetry. The spin-3/2 states are the "heavy-hole" states and the spin-1/2 states are the "light-hole" states. The requirement that we take the projection of the valence-band state onto the same spin state as the conduction-band state, for the eight exciton states listed in Appendix A, gives us the set of coefficients

$$\begin{pmatrix}
1 & 0 & 0 & 0 & 0 & 0 & 0 & 0 \\
0 & 0 & -\frac{4}{\sqrt{3}} & 0 & 0 & 0 & 0 & 0 \\
0 & -\frac{4}{\sqrt{3}} & \frac{2}{3} & 0 & 0 & 0 & 0 & 0 \\
0 & 0 & 0 & \frac{1}{3} & \frac{4}{3} & 0 & 0 & 0 \\
0 & 0 & 0 & \frac{4}{3} & \frac{1}{3} & 0 & 0 & 0 \\
0 & 0 & 0 & 0 & 0 & \frac{2}{3} & -\frac{4}{\sqrt{3}} & 0 \\
0 & 0 & 0 & 0 & 0 & -\frac{4}{\sqrt{3}} & 0 & 0 \\
0 & 0 & 0 & 0 & 0 & 0 & 0 & 1
\end{pmatrix}. \tag{B9}$$

This is the same result as obtained using $\frac{1}{2}\vec{S}_e \cdot \vec{S}_h + \frac{1}{2}$, which is the same as the matrix in Eq. (A6) in Appendix A, except for the additive constant, for the case $a_x = a_y = a_z$. This shows that at a fundamental level, the electron-hole exchange splitting term is proportional to $\vec{S}_e \cdot \vec{S}_h$, not $\vec{S}_e \cdot \vec{J}_h$, which does not give an equivalent matrix.

In a quantum well and under shear stress, the p states $|1\rangle$, $|0\rangle$, and $|-1\rangle$ are no longer the orbital eigenstates, as x, y, and z are no longer equivalent. The new eigenstates become $|x\rangle = \frac{1}{\sqrt{2}}(|-1\rangle - |1\rangle)$, $|y\rangle = \frac{i}{\sqrt{2}}(|-1\rangle + |1\rangle)$ and $|z\rangle = |0\rangle$. When these are used in Eq. (B5), the values of the coefficients a_x, a_y, and a_z can be obtained.

*Present address: Iligan Institute of Technology, Mindanao State University, 9200 Iligan City, Philippines.
†snoke@pitt.edu
‡Present address: Department of Electrical Engineering, Princeton University, Princeton, NJ 08544, USA.

[1] S. Savasta, O. DiStefano, V. Savona, and W. Langbein, Phys. Rev. Lett. **94**, 246401 (2005).
[2] T. C. H. Liew, Y. G. Rubo, and A. V. Kavokin, Phys. Rev. Lett. **101**, 187401 (2008).
[3] S. Christopoulos, G. Baldassarri Höger von Högersthal, A. Grundy, P. G. Lagoudakis, A. V. Kavokin, J. J. Baumberg, G. Christmann, R. Butté, E. Feltin, J.-F. Carlin, and N. Grandjean, Phys. Rev. Lett. **98**, 126405 (2007).
[4] R. Shimada, J. Xie, V. Avrutin, U. Ozgur, and H. Morkoc, Appl. Phys. Lett. **92**, 011127 (2008).
[5] C. Leyder, T. C. H. Liew, A. V. Kavokin, I. A. Shelykh, M. Romanelli, J. Ph. Karr, E. Giacobino, and A. Bramati, Phys. Rev. Lett. **99**, 196402 (2007).
[6] S. Kundermann, M. Saba, C. Ciuti, T. Guillet, U. Oesterle, J. L. Staehli, and B. Deveaud, Phys. Rev. Lett. **91**, 107402 (2003).
[7] J. Keeling, P. R. Eastham, M. H. Szymańska, and P. B. Littlewood, Phys. Rev. Lett. **93**, 226403 (2004).
[8] J. Kasprzak, M. Richard, S. Kundermann, A. Baas, P. Jeambrun, J. M. J. Keeling, R. Andre, J. L. Staehli, V. Savona, P. B. Littlewood, B. Deveaud, and L. S. Dang, Nature (London) **443**, 409 (2006).
[9] R. Balili, V. Hartwell, D. Snoke, L. Pfeiffer, and K. West, Science **316**, 1007 (2007).
[10] J. J. Baumberg, A. V. Kavokin, S. Christopoulos, A. J. D. Grundy, R. Butté, G. Christmann, D. D. Solnyshkov, G. Malpuech, G. Baldassarri Höger von Högersthal, E. Feltin, J.-F. Carlin, and N. Grandjean, Phys. Rev. Lett. **101**, 136409 (2008).
[11] A. Baas, K. G. Lagoudakis, M. Richard, R. André, Le Si Dang, and B. Deveaud-Plédran, Phys. Rev. Lett. **100**, 170401 (2008).
[12] A. P. D. Love, D. N. Krizhanovskii, D. M. Whittaker, R. Bouchekioua, D. Sanvitto, S. Al. Rizeiqi, R. Bradley, M. S. Skolnick, P. R. Eastham, R. André, and L. S. Dang, Phys. Rev. Lett. **101**, 067404 (2008).
[13] K. Lagoudakis, M. Wouters, M. Richard, A. Baas, I. Carusotto, R. Andr, Le Si Dang, and B. Deveaud-Pldran, Nat. Phys. **4**, 706 (2008).
[14] A. Amo, D. Sanvitto, F. P. Laussy, D. Ballarini, E. del Valle, M. D. Martin, A. Lemaitre, J. Bloch, D. N. Krizhanovskii, M. S. Skolnick, C. Tejedor, and L. Viña, Nature (London) **457**, 291

(2009).
[15] D. Bajoni, P. Senellart, E. Wertz, I. Sagnes, A. Miard, A. Lemaitre, and J. Bloch, Phys. Rev. Lett. **100**, 047401 (2008).
[16] R. Balili, B. Nelsen, D. W. Snoke, L. Pfeiffer, and K. West, Phys. Rev. B **79**, 075319 (2009).
[17] C. Lai, N. Y. Kim, S. Utsunomiya, G. Roumpos, H. Deng, M. D. Fraser, T. Byrnes, P. Recher, N. Kumada, T. Fujisawa, and Y. Yamamoto, Nature (London) **450**, 529 (2007).
[18] H. Deng, G. Weihs, C. Santori, J. Bloch, and Y. Yamamoto, Science **298**, 199 (2002).
[19] V. Negoita, D. W. Snoke, and K. Eberl, Appl. Phys. Lett. **75**, 2059 (1999).
[20] H. Deng, G. Weihs, D. Snoke, J. Bloch, and Y. Yamamoto, Proc. Natl. Acad. Sci. U.S.A. **100**, 15318 (2003).
[21] E. Blackwood, M. J. Snelling, R. T. Harley, S. R. Andrews, and C. T. B. Foxon, Phys. Rev. B **50**, 14246 (1994).
[22] N. Romanov and P. Baranov, Nanotechnology **12**, 585 (2001).
[23] R. Balili, D. Snoke, L. Pfeiffer, and K. West, Appl. Phys. Lett. **88**, 031110 (2006).
[24] O. Berman, Y. Lozovik, and D. Snoke, Phys. Status Solidi **3**, 3373 (2006).
[25] E. L. Ivchenko, A. Y. Kaminski, and U. Rössler, Phys. Rev. B **54**, 5852 (1996).
[26] S. Jorda, U. Rössler, and D. Broido, Phys. Rev. B **48**, 1669 (1993).
[27] R. Seguin, A. Schliwa, S. Rodt, K. Potschke, U. W. Pohl, and D. Bimberg, Physica E **32**, 101 (2006).
[28] H. W. van Kesteren, E. C. Cosman, W. A. J. A. van der Poel, and C. T. Foxon, Phys. Rev. B **41**, 5283 (1990).
[29] K. Cho, Phys. Rev. B **14**, 4463 (1976).
[30] L. Klopotowski, M. D. Martin, A. Amo, L. Viña, I. A. Shelykh, M. M. Glazov, G. Malpuech, A. V. Kavokin, and R. André, Solid State Commun. **139**, 511 (2006).
[31] Z. Vörös, Ph.D. thesis, University of Pittsburgh, 2008.
[32] E. Ivchenko and G. Pikus, *Superlattices and Other Heterostructures*, 2nd. ed. (Springer, Berlin, 1997); E. L. Ivchenko, *Optical Spectroscopy of Semiconductor Nanostructures* (Alpha Science International, Oxford, UK 2005), p. 258.
[33] M. Bayer, G. Ortner, O. Stern, A. Kuther, A. A. Gorbunov, A. Forchel, P. Hawrylak, S. Fafard, K. Hinzer, T. L. Reinecke, S. N. Walck, J. P. Reithmaier, F. Klopf, and F. Schäfer, Phys. Rev. B **65**, 195315 (2002).
[34] S. Chuang, *Physics of Optoelectronic Devices* (Wiley, New York, 1995), Appendices J and K.
[35] R. I. Cottam and G. A. Saunders, J. Phys. C **6**, 2105 (1973).
[36] P. Y. Yu and M. Cardona, *Fundamentals of Semiconductors*, 3rd ed. (Springer, Berlin, 1996), p. 119.
[37] J. S. Blakemore, J. Appl. Phys. **53**, R123 (1982).
[38] D. Snoke, *Solid State Physics: Essential Concepts* (Addison-Wesley, San Francisco, 2009).
[39] E. Hanamura and H. Haug, Phys. Rep. **33**, 209 (1977).